Semi–numerical Simulation of a Miniaturized Vibrating Membrane–Rheometer

Thomas Voglhuber–Brunnmaier, Erwin Konrad Reichel, Bernhard Jakoby
Institute for Microelectronics and Microsensors
Johannes Kepler University
Altenbergerstr. 69, 4040 Linz, Austria

Introduction

For online process monitoring purposes micro–rheometers based upon quartz resonators are commonly used but suffer from weak comparability of the results compared to those obtained from traditional laboratory viscometers [1]. This discrepancy is partly explained by the low agitation of the measured liquid within these micro–rheometers – this issue is addressed by a larger deformation at lower frequencies in our present measurement setup. In our contribution we investigate a miniaturized clamped membrane device as shown in Fig. 1 (left). This system consists of a sample cell of $5.6 \times 12 \times 1$ mm^3 size filled with the liquid under test. Its bottom and top side both are sealed by 52 µm thick PMMA-membranes which are excited to vibrations. For the analysis of this problem finite element (FE) solvers fail due to the large amount of elements required for adequate discretization. The viscosity coefficient of the liquid under test is linearly related to the power dissipation due to shear velocity gradients in the sample fluid which causes a finite Q–factor of the resonance peak. Fig. 1 (right) shows that moreover considerable gradients do mainly occur within a thin – tens of microns – layer close to the membrane–fluid interface. Therefore a FE discretization of the outermost liquid regions would have to be sufficiently fine as well.

In the presented contribution the problem of high numerical complexity is addressed using an alternative approach, namely a semi–numerical representation in the spectral domain. The membranes are described by using equations of motion and the constitutive equations of linear visco–elastic bulk material. The fluid sample volume is modeled employing Navier–Stokes equations, which can be linearized in case of the present problem (as will be discussed in the paper). The description of the fluid includes first and second viscosity coefficients and pressure–density coupling via compressibility coefficient as well. Our approach is based upon the conversion of the thus obtained partial differential equations (PDEs) to ordinary differential equations (ODEs) by expressing the field variables (displacements and stresses) by a harmonic representation in the spectral domain [2]. This yields two Eigenvalue problems – one for the membranes and one for the fluid. The computational effort is reduced drastically this way. The principle solution of the obtained Eigenvalue problem describing the fluid is coupled to the membrane equations by means of a propagator matrix, which is derived from the solution of the Eigenvalue problem of the membrane. Taking into account boundary conditions and rearranging the solution system finally leads to the frequency response of the sensor. By analyzing the frequency response in the vicinity of the resonance peak, a behaviour similar to a damped second order system is revealed. The numerically found frequency response is compared to experimental results obtained with the micro–rheometer shown in Fig. 1 (left). For time–harmonic excitation of the membranes via Lorentz forces conductive paths are patterned. Read–out is also achieved by a further pair of conductive paths. Imposed forces result in time-harmonic displacements which induce voltages in the read–out path. The frequency response showing dependency to liquid and membrane properties is measured by a lock–in amplifier setup. In the following sections the model is outlined in detail and numerical sample results are presented.

Modeling of the membranes

According to the linear visco–elastic properties of solids described by the Voigt–Kelvin model [3], the relation between the stress tensor $\boldsymbol{T}$ and the strain tensor $\boldsymbol{S}$ is given by $\boldsymbol{T} = \boldsymbol{c} \cdot \boldsymbol{S} + \boldsymbol{\eta} \cdot \partial \boldsymbol{S}/\partial t$, where $\boldsymbol{c}$ and $\boldsymbol{\eta}$ denote stiffness and damping tensor of the considered solid[1]. The equation of motion for linear visco–elastic deformations expressed in terms of stresses $\boldsymbol{T}$ and displacements $\boldsymbol{u}$ without external forces is given by

$$\rho_s \frac{\partial^2 \boldsymbol{u}}{\partial t^2} = \nabla \cdot \boldsymbol{T}, \tag{1}$$

[1] An element in row k and column l of the linear strain tensor is given by $S_{kl} = 1/2\,(\partial u_k/\partial x_l + \partial u_l/\partial u_k)$ with u_k denoting the k^{th} displacement component

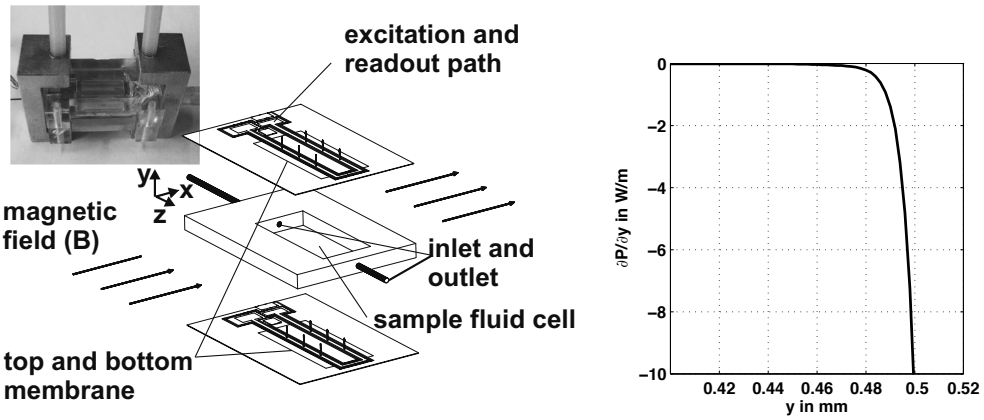

Figure 1: Photograph and schematic of the sensor. The membranes carry conductive paths for excitation by Lorentz forces. Separate paths are used for read–out (left). The calculated energy dissipation in the fluid in layers at y is shown right. Main dissipation occurs close to the membranes (at $y = \pm 0.5$mm).

where ρ_s denotes the mass density of the membrane material[2]. Substitution of Hooke's law into Eqn. 1 yields a system of PDEs describing the behaviour of a linear bulk material. Introducing Lame's constants μ_s and λ_s and their lossy equivalents – shear viscosity coefficient μ_s' and volume viscosity coefficient λ_s' – Eqn. 2 can be obtained[3].

$$\rho_s \ddot{\boldsymbol{u}} = (\mu_s + \mu_s' \frac{\partial}{\partial t}) \nabla^2 \boldsymbol{u} + \left((\lambda_s + \mu_s) + (\lambda_s' + \mu_s') \frac{\partial}{\partial t} \right) \nabla (\nabla \cdot \boldsymbol{u}) \tag{2}$$

Modeling the fluid cell

The equations of motion of a viscous fluid without considering external forces are provided by the Navier–Stokes equations and by the continuity equation, given in Eqn. 3 and Eqn. 4 (see [4]).

$$\rho_f (\ddot{\boldsymbol{u}} + (\dot{\boldsymbol{u}} \cdot \nabla) \dot{\boldsymbol{u}}) = -\nabla p + \mu_f' \nabla^2 \dot{\boldsymbol{u}} + (\lambda_f' + \mu_f') \nabla (\nabla \cdot \dot{\boldsymbol{u}}) \tag{3}$$

$$\frac{\partial \rho_f}{\partial t} + \nabla \cdot (\rho_f \dot{\boldsymbol{u}}) = 0 \tag{4}$$

The considered velocities are assumed to be small and time–harmonic. Thus the nonlinear convective part of Eqn. 3 $(\dot{\boldsymbol{u}} \cdot \nabla) \dot{\boldsymbol{u}}$ may be neglected[4]. A coupling between pressure p and mass density ρ_f is achieved using the adiabatic compressibility coefficient $\zeta = \rho^{-1} (\partial \rho_f / \partial p)$. Assuming small deviations p and $\rho_{f,e}$ from the equilibrium p_0 and $\rho_{f,0}$, Eqn. 3 and Eqn. 4 can be rewritten [1] as.

$$\rho_f \ddot{\boldsymbol{u}} = \frac{1}{\zeta} \nabla (\nabla \cdot \boldsymbol{u}) + \mu_f' \nabla^2 \dot{\boldsymbol{u}} + (\lambda_f' + \mu_f') \nabla (\nabla \cdot \dot{\boldsymbol{u}}) \tag{5}$$

The spectral domain method

In stratified sensor geometries dependencies of field variables along the axis of stratification – in our problem the z–axis – can often be neglected, and a 2D simulation of the sensor is sufficient. Due to a periodic approximation outlined in the following, the method can be readily applied to model the fields in the fluid cell. The linear problem in Eqn. 5 contains no mixed derivatives which may be solved using a separated solution ansatz $\boldsymbol{\psi}(x, y, t) = \boldsymbol{\psi_y}(y) \cdot \psi_x(x) \cdot \psi_t(t)$[5]. We introduce a partial spatial spectral Fourier transform, where ω denotes the angular frequency of the time–harmonic part and k_x is the wave number associated to the harmonic spatial term in x–direction:

$$\boldsymbol{\psi}(x, y, t) = \boldsymbol{\psi_y}(y) \cdot \frac{1}{4\pi^2} \int_{-\infty}^{\infty} \int_{-\infty}^{\infty} \Psi_\omega(\omega) \Psi_{k_x}(k_x) \exp(j k_x x - j \omega t) dk_x d\omega. \tag{6}$$

The linearity of the stated problem allows to solve Eqn. 5 for given frequencies ω and wave numbers k_x and to superpose the solutions with adequate weighting functions $\Psi_{k_x}(k_x)$ and $\Psi_\omega(\omega)$:

[2] In the remainder of this paper, the subscript s refers to solids.

[3] Lame's constants are provided by $\mu_s = E_s/(2(1+\nu_s))$ and $\lambda_s = E_s \nu_s / ((1+\nu_s)(1-2\nu_s))$ with Young's modulus E_s and Poisson's ratio ν_s [6]

[4] The contribution of the convective part is on the order of 10^{-3} compared to linear terms which is proved by resubstitution of the calculated velocity field.

[5] The vector $\boldsymbol{\psi}(x, y, t)$ contains the field variables describing the problem.

$$\boldsymbol{\psi}(x,y,t) = \frac{1}{4\pi^2}\int_{-\infty}^{\infty}\int_{-\infty}^{\infty}\Psi_{k_x}(k_x)\Psi_{\omega}(\omega)\boldsymbol{\phi}(k_x,y,\omega)dk_x d\omega \tag{7}$$

For further derivations, a single spectral case $\boldsymbol{\phi}(x,y,t)$ of this spectrum is considered:

$$\boldsymbol{\phi}(k_x,y,\omega) = \boldsymbol{\psi}_y(y)\cdot\exp(jk_x x - j\omega t) \tag{8}$$

By substituting the ansatz from Eqn. 8 into Eqs. 1 and 5, the PDEs describing the membranes and the fluid cell are transformed into two systems of second order ODEs. An obvious selection of representative field variables would consist of the displacement vector $\boldsymbol{u} = [u_x, u_y]^T$ and its derivative with respect to y. However for the considered sensor geometry (Fig. 1) it is more advantageous to replace the derivatives with stresses. In the planar case the stress tensor consists of three values T_{xx}, T_{xy}, T_{yy}, but only two of them suffice to describe the stress situation, as these values are not independent (see Mohr's circle [6]). We chose shear stress T_{xy} and normal stress T_{yy} as they are imposed at the top of the membranes. The resulting field variables are thus written as

$$\boldsymbol{\phi}(k_x,y,\omega) = [u_x(y), u_y(y), T_{xy}(y), T_{yy}(y)]^T\cdot\exp(jk_x x - j\omega t), \tag{9}$$

and the obtained system of first order ODEs of rank 4 describing the membranes considering Eqn. 8 is

$$\frac{\partial}{\partial y}\boldsymbol{\phi}(k_x,y,\omega) = \boldsymbol{A_s}\boldsymbol{\phi}(k_x,y,\omega), \qquad \frac{\partial}{\partial y}\boldsymbol{\psi_y}(y) = \boldsymbol{A_s}\boldsymbol{\psi_y}(y). \tag{10}$$

In a completely analogous manner the system describing the fluid layer is found as $\frac{\partial}{\partial y}\boldsymbol{\psi_y}(y) = \boldsymbol{A_f}\boldsymbol{\psi_y}(y)$. The general solution of the Eigenvalue problem shown in Eqn. 10 is given by Eqn. 11 as

$$\boldsymbol{\psi_y}(y) = \exp(\boldsymbol{A_s}y)\cdot\boldsymbol{c} = c_1\boldsymbol{v_1}\exp(\lambda_1 y) + c_2\boldsymbol{v_2}\exp(\lambda_2 y) + c_3\boldsymbol{v_3}\exp(\lambda_3 y) + c_4\boldsymbol{v_4}\exp(\lambda_4 y) \tag{11}$$

with $\boldsymbol{v_1}\cdots\boldsymbol{v_4}$, $\lambda_1\cdots\lambda_4$ denoting Eigenvectors and Eigenvalues of the system matrix $\boldsymbol{A_s}$. The constants $\boldsymbol{c} = [c_1\cdots c_4]^T$ have to be set according to adequate boundary conditions. A similar solution is obtained for the fluid layer. The structure of the system matrices $\boldsymbol{A_s}$ and $\boldsymbol{A_f}$ describing visco–elastic material and the fluid layer imply $\lambda_2 = -\lambda_1$ and $\lambda_4 = -\lambda_3$ and Eqn. 12 regarding the Eigenvectors $\boldsymbol{v_1}$ to $\boldsymbol{v_4}$.

$$\boldsymbol{v_1} = \begin{bmatrix} v_{11}\\ v_{12}\\ v_{13}\\ v_{14}\end{bmatrix}, \boldsymbol{v_2} = \begin{bmatrix} -v_{11}\\ v_{12}\\ v_{13}\\ -v_{14}\end{bmatrix}, \boldsymbol{v_3} = \begin{bmatrix} v_{31}\\ v_{32}\\ v_{33}\\ v_{34}\end{bmatrix}, \boldsymbol{v_4} = \begin{bmatrix} -v_{31}\\ v_{32}\\ v_{33}\\ -v_{34}\end{bmatrix}. \tag{12}$$

Boundary conditions

The Lorentz forces apply stresses in y-direction to the conductive paths on top of the membranes. The velocity of the resulting excitation of the membranes is measured by the read out paths of the sensor. To calculate the displacement vector $\boldsymbol{u}$ and the stresses at any layer y of the sensor we have to determine the four constants $[c_1\ldots c_4]$ according to the given boundary conditions. This could be achieved by solving Eqn. 11 for the constants at a position y_0 if $\boldsymbol{\psi_y}(y_0)$ were known. Unfortunately in our case this is not possible since only the stresses T_{yy} and T_{xy} are known at two positions $\pm y_b = \pm(d_m + f_f/2)$. Due to linearity, any stress distribution on top and bottom membrane may be imposed by superposing the two principal excitation modes – symmetric (excitation of top membrane in $+y$ and bottom membrane in $-y$ direction) or anti–symmetric (top and bottom membrane equally directed see also Fig. 2). For both cases we consider the symmetry relations given in Fig. 2. Employing these symmetry relations we obtain Eqn. 13.
These equations can be used to describe the field within the liquid. The unknown coefficients $[c_1\cdots c_4]$ have to be determined from the boundary conditions at the membranes.

$$\begin{bmatrix} u_x(y)\\ u_y(y)\\ T_{xy}(y)\\ T_{yy}(y)\end{bmatrix} = \underbrace{\frac{1}{2}\begin{bmatrix} v_{11}\cosh(\lambda_1 y) & v_{31}\cosh(\lambda_3 y)\\ v_{12}\sinh(\lambda_1 y) & v_{32}\sinh(\lambda_3 y)\\ v_{13}\sinh(\lambda_1 y) & v_{33}\sinh(\lambda_3 y)\\ v_{14}\cosh(\lambda_1 y) & v_{34}\cosh(\lambda_3 y)\end{bmatrix}}_{\boldsymbol{E_{sym}}}\begin{bmatrix} c_1\\ c_3\end{bmatrix}, \begin{bmatrix} u_x(y)\\ u_y(y)\\ T_{xy}(y)\\ T_{yy}(y)\end{bmatrix} = \underbrace{\frac{1}{2}\begin{bmatrix} v_{11}\sinh(\lambda_1 y) & v_{31}\sinh(\lambda_3 y)\\ v_{12}\cosh(\lambda_1 y) & v_{32}\cosh(\lambda_3 y)\\ v_{13}\cosh(\lambda_1 y) & v_{33}\cosh(\lambda_3 y)\\ v_{14}\sinh(\lambda_1 y) & v_{34}\sinh(\lambda_3 y)\end{bmatrix}}_{\boldsymbol{E_{asym}}}\begin{bmatrix} c_1\\ c_3\end{bmatrix} \tag{13}$$

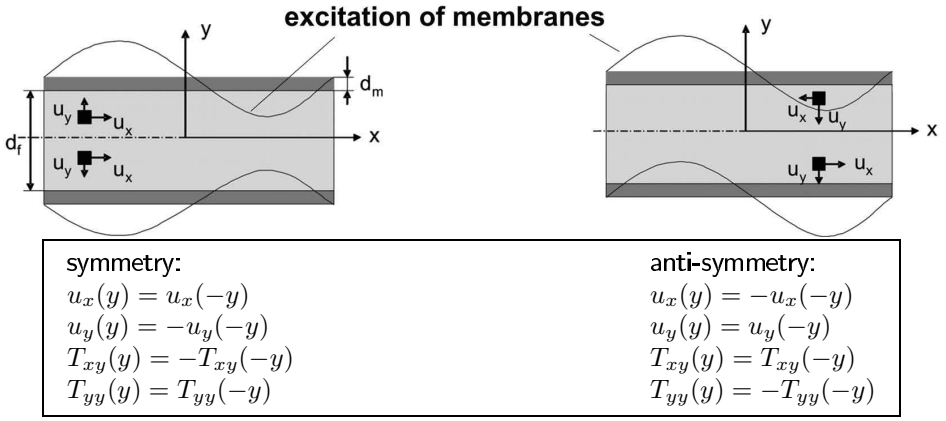

Figure 2: Symmetry relations for the two principle excitation modes.

Propagation of field variables

The field within the membranes can also be described in spectral domain by Eqn. 10. However, we now integrate Eqn. 10 with respect to y to obtain a relation between $\boldsymbol{\psi_y}(y)$ at two faces of the membrane, the so–called propagator matrix $\boldsymbol{P}$ [2]:

$$\boldsymbol{\psi_y}(d_f/2) = \boldsymbol{P}(-dm) \cdot \boldsymbol{\psi_y}(d_f/2 + dm). \tag{14}$$

As all components of $\boldsymbol{\psi_y}(y)$ are continuous at the interface $y = d_f/2$, we can write, e.g. for the symmetric mode

$$\boldsymbol{\psi_y}(y_b) = \boldsymbol{P_s}(d_m) \cdot \boldsymbol{\psi_y}(d_f/2) = \boldsymbol{P_s}(d_m) \cdot \boldsymbol{E_{sym}}(d_f/2) \cdot \begin{bmatrix} c_1 \\ c_3 \end{bmatrix} \tag{15}$$

As T_{yy} and T_{xy} are prescribed at y_b, we can obtain c_1 and c_3 and hence the entire field distribution.

Actuation

The implemented routing of conductive paths is shown in Fig. 4. The read–out path consists of several loops to increase the output voltage level. The excitation path is routed to achieve anti–symmetric excitation of top and bottom membrane. The imposed stress T_{yy} has rectangular shape and yields a continuous spectrum after a spatial Fourier transform (see Eqn. 7). To avoid dealing with an infinite spectrum we approximate the problem by considering a periodic problem where the interval $x = (-L/2, L/2)$ represents the fundamental period. The continuous spectrum thus reduces to a discrete spectrum or Fourier series. However, this means that we can not fix any field variables at the boundary at $x = \pm L/2$ which implies that we can not apply the no–slip condition at these boundaries. As this discrepancy is mainly restricted to regions near the boundary at $x = \pm L/2$ the obtained results still are valid for the complete setup. As for the time domain we consider time–harmonic excitation. Hence it is sufficient to consider the associated spectral line ω.

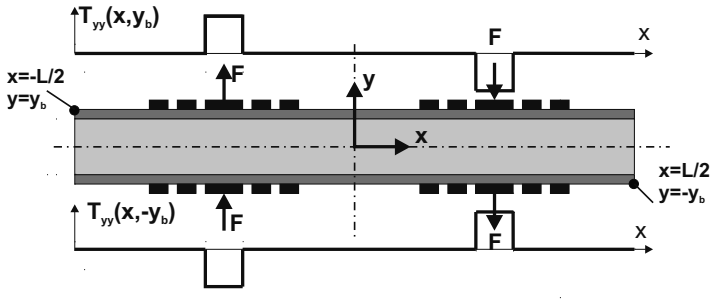

Figure 3: Normal stress distribution and Lorentz forces $\boldsymbol{F}$ on top and bottom membrane.

Definition of the transfer function

The stresses $T_{yy}(y_b)$ and $T_{yy}(-y_b)$ are imposed by Lorentz excitation and the shear stresses $T_{xy}(y_b)$ and $T_{xy}(-y_b)$ are assumed to be zero as air friction is neglected. In Fig. 5 a displacement field simulated with the presented

method is shown. For the assumed linear problem, a transfer function relating input and output can be found. The output signal U_{ind} is the voltage induced in the read–out path, being proportional to the external magnetic induction $\boldsymbol{B}$ with amplitude B, length l perpendicular to $\boldsymbol{B}$ and the membrane top velocity $\partial u_y/\partial t$ at $\pm y_b$. The input signal I_{exc} is a current driven through the excitation path forming a force proportional to current and magnetic induction $\boldsymbol{B}$. The desired transfer function thus turns out to be an impedance $Z(\omega)$ given in Eqn. 16. Summing up the contributions of all paths at $x = [l_{r1} \cdots l_{r4}]$, we obtain (see also Fig. 4:

$$Z(\omega) = \frac{U_{ind}}{I_{exc}} - 4\frac{j\omega B^2}{b}\frac{\sum_{x=l_{r1}}^{l_{r4}} u_y(x, y_b, \omega)}{T_{yy}(l_e, y_b, \omega)}. \tag{16}$$

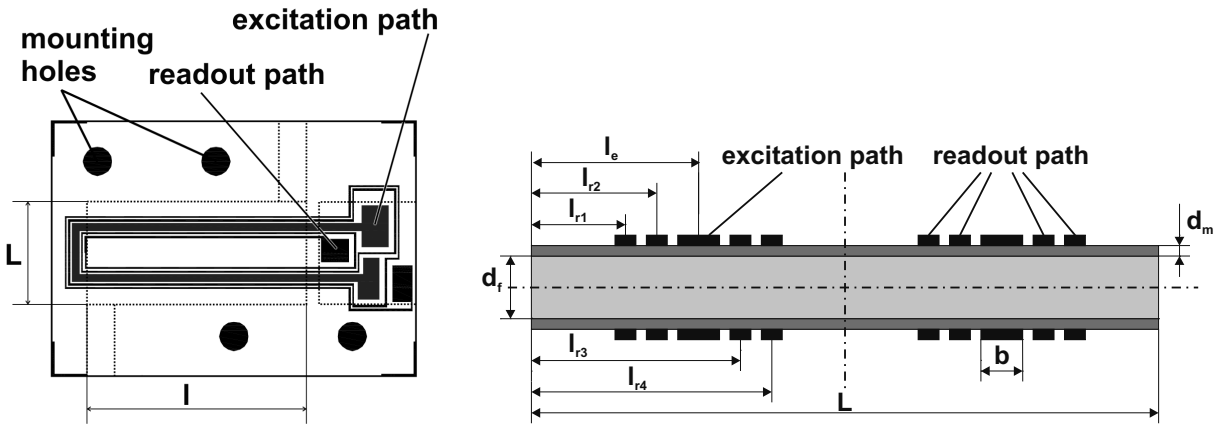

Figure 4: Implemented routing of the conductive paths on membrane top (left), and cross section through the sensor cell showing path geometry (right).

Discussion and Conclusions

Fig. 5 shows the simulated displacement field for a 55% glycerine–water mixture at $\omega = 320s^{-1}$ and displacement component[6] u_x at $x = 0$. The simulated velocity field is shown in Fig. 6. The velocity component $v_x = \dot{u}_x$ at $x = 0$ show that high velocity gradients – responsible for energy loss due to viscous friction – do mainly occur close the membranes. The total energy loss in the fluid sample cell can be approximated using relation[7]

$$P = -\frac{\mu'_f}{2}\int_V \left(\frac{\partial v_i}{\partial x_j} + \frac{\partial v_j}{\partial x_i}\right)^2 dV \tag{17}$$

The energy loss in any layer of width dy at y is shown in Fig. 1 (right). Fig. the simulated membrane top displacement and measurement results obtained by lock–in amplifiers and Eqn. 16 are compared for three different mixtures. The model describes the measurement reasonably well, the deviations can be related to unequal clamping support of top and bottom membrane (which is not contained in the model) and insufficient calibration of the measurement setup (phase errors). Measurement results obtained with the current setup showed that the viscosity range of liquids under test is limited. The presented simulation method helped adapting setup parameters like fluid cell height, membrane thickness, and mixture ratio of symmetric and anti-symmetric excitation mode to achieve sensor designs working well in the desired range of the viscosity and density coefficient of the liquids under test.

[6] Viscosity coefficient and density are $\mu'_f = 7.2e^{-3}$ Pa s and $\rho_f = 1139$ kg/m^3.

[7] This relation is valid for incompressible flow. Energy dissipation due to the 2nd viscosity coefficient is considered neglectable.

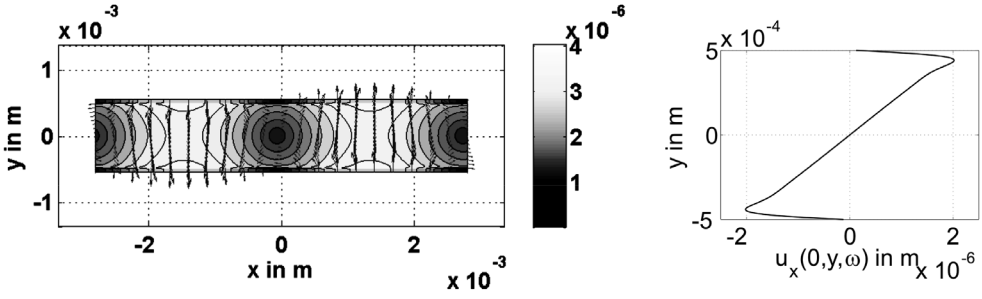

Figure 5: Simulated displacement field (left) and displacement component u_x at $x = 0$ (right) for a 55% glycerine–water mixture.

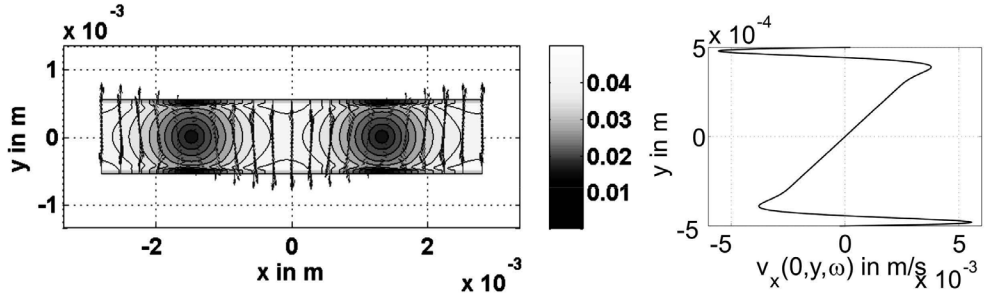

Figure 6: Simulated velocity field (left) and velocity component $\dot{u}_x$ at $x = 0$ (right) for a 55% glycerine–water mixtrure.

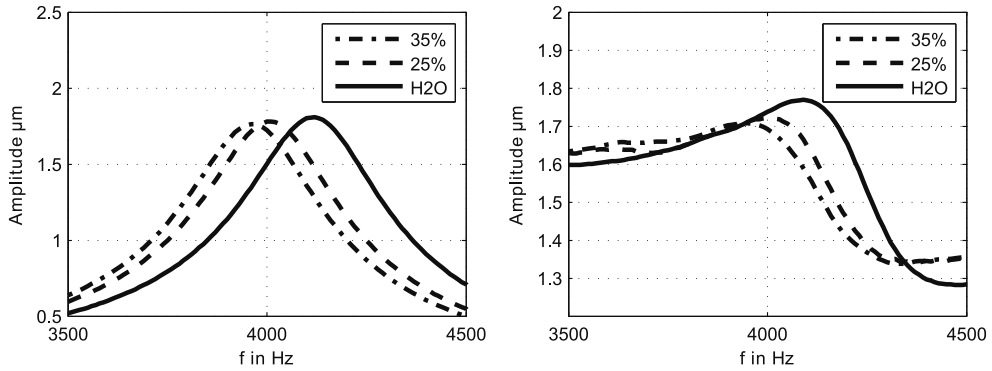

Figure 7: Frequency response (displacement at thef membrane top) for three different mixtures of water and glycerine acquired with the current setup.

References

[1] E.K. Reichel, B. Weiß, B. Jakoby, A Novel Micromachined Liquid Property Sensor Utilizing A Doubly Clampled Vibrationg Beam, Proc. Eurosensors XX Göteborg, 2006

[2] B. Jakoby, Efficient semi-numerical analysis of acoustic sensors using spectral domain methods – a review – Measurement Science and Technology, vol. 19,

[3] S.L. Rosen, Fundamental Principles of Polymeric Materials, John Wiley & Sons, Inc., 1993

[4] L.D. Landau, E.M. Lifshitz, Fluid Mechanics, 2nd Edition, Pergamon Press 1987

[5] E.K. Reichel, C. Riesch, F. Keplinger, B. Jakoby, Resonant Measurement of Liquid Properties in a Fluidic Sensor Cell, Proc. Eurosensors XXII Dresden, 2008

[6] F. Ziegler, Mechanics of Solids and Fluids, Springer, 1991 2008, pp 052001, IOP Publishing, 2008